Shaking table test on a segmental tunnel crossing strike-slip active fault

Huihui Hu, Shuo Li
Department of Geotechnical Engineering, Tongji University, Shanghai 200092, China, 2510063@tongji.edu.cn, 2330985@tongji.edu.cn

Haitao Yu
State Key Laboratory of Disaster Reduction in Civil Engineering, Tongji University, Shanghai 200092, China, yuhaitao@tongji.edu.cn

ABSTRACT: Mountain tunnels traversing active faults face significant damage risks due to the complex coupling effect of ground motion and coseismic dislocation. However, existing physical model tests have been limited to investigating ground motion or dislocation individually, or their sequential application, leaving a critical gap in understanding their simultaneous coupling effect. To address this, we conducted an innovative model test using a specially developed multi-layer linkage coupling device integrated with Tongji University's multi-point shaking table system. This setup enables the synchronous application of seismic shaking and fault dislocation. The scaled model satisfies similitude relations for both ground-tunnel relative stiffness and strength. The model tunnel, fabricated with custom formwork, accurately replicates the three-center arch circle section, segmental joints, and longitudinal joint stiffness reductions. Testing commenced with a free-field model to characterize ground response and fault rupture propagation using optical frequency domain reflectometry (OFDR) sensing. Subsequently, the ground-tunnel model test focused on soil-structure interaction, tunnel dynamic response and alignment, and lining/joint deformations. This study provides a basis for assessing tunnel performance under simultaneous seismic and fault dislocation conditions.

1 INTRODUCTION

Physical model tests for tunnels crossing active faults are typically conducted to simulate and analyze the structural behaviour and response of tunnels under the combined action of fault movement and other potential loads. The complex kinematic characteristics and unique structural features of the fault directly influence the stress and deformation behaviour of the tunnel structure. Therefore, the core of test design lies in recreating the fault's movement and deformation mechanisms through rational model fabrication and loading scheme design, thereby achieving an effective simulation of the active fault, ensuring the scientific rigor of the test and the accuracy of the results.

Currently, physical experimental research on tunnels crossing active faults can be primarily categorized into three types based on the applied loads: applying ground motion only, applying fault dislocation only, and applying fault dislocation followed by ground motion. These can be further subdivided according to the type of ground motion (the input direction; with/without velocity pulse characteristics), the type of fault dislocation (normal /reverse/strike-slip fault; creep or stick-slip), and the method of simulating the fault structure.

Based on the literature reviews, it is evident that simulating active faults in shaking table tests for tunnels crossing active faults presents two key challenges: the simulation of the fault's kinematic characteristics and the simulation of the fault's structural features.

1.1 Fault kinematic characteristics

Zhang et al. (2023) simulated uniformly distributed fault rupture surfaces by filling a 1cm-thick mixture of river sand and sawdust at three equal-division points on both sides and within the fault zone. Rollers were installed on the steel plate at the bottom of the fault zone. When horizontal transverse ground motion was input, the fault zone experienced transverse displacement relative to the hanging wall and footwall, simulating the activation of secondary fractures induced by earthquakes. Liu et al. (2019) simulated the sequential arrival of P-waves and S-waves at an active fault during an actual earthquake by first applying S-waves vibrating along the tunnel axis, followed by P-waves vibrating vertically with a peak value about one-third of the former. Shen et al. (2020) first used jacks to lift the tunnel's hanging wall, then placed the surrounding rock model material and installed the model tunnel. During loading, all jacks were released simultaneously, allowing the hanging wall to move downward under gravity to simulate normal fault stick-slip dislocation, after which horizontal transverse ground motion was applied. This process simulated the scenario where a significant fault dislocation is immediately followed by an earthquake.

However, in seismically active regions with high intensity, the coupled action of active fault dislocation and strong earthquakes on tunnels may also occur. Physical test loading methods for such scenarios remain rarely studied.

1.2 Fault's structural features

Due to the diverse structure of fault zones and limitations in test conditions, the simulation methods for fault structure vary significantly across different studies. Considering that the hanging wall and footwall in their model were Class IV and Class V surrounding rock respectively, with significant property differences, Xu and Li (2022) used a PVC plate to separate them and applied butter between the plates to simulate fault dislocation—a simple and practical method. Xu et al. (2016) simulated the fault by laying a certain thickness of talcum powder, allowing the fault thickness and the friction coefficient of the contact surface in the model to meet similarity conditions. Xin et al. (2016) and Wang et al. (2015) both used gravel with low cohesion to simulate the surrounding rock of the fault zone and laid polyethylene plastic film between the fault zone and the hanging wall/footwall surrounding rock to reduce friction. The simulations of the fault zone in the above studies primarily focused on the similarity design of its geometric features and the frictional characteristics of the sliding surface, appropriately relaxing the similarity requirements for the physical properties of the rock within the broken zone. Sun et al. (2018) considered the surrounding rock within the fault zone as Class V, taking into account parameters such as unit weight, elastic modulus, and cohesion when preparing the similar materials. The simulated fault width was 27 m, but the existence of a fault rupture surface was not considered.

This study select a railway tunnel located in Southwest China injected through a sinistral strike-slip active fault as the prototype. This active fault zone has a width of 180 m. The rock mass quality grades from the hanging wall to the footwall are Class V1, Class V2, Class VI, Class V2, and Class IV, respectively. Based on the latest survey results of active faults and historical earthquake statistics, there are 49 potential seismic source zones of M ≥ 7.0 along the route and in the surrounding area, and 2 earthquakes of M ≥ 8.0 have occurred in the past century. Therefore, strong motion-dislocation coupled ground motions (with post-earthquake residual displacement) should be imposed to the hanging wall and footwall respectively during the loading phase to achieve simulation of the co-seismic dislocation condition. The front view of the shaking table model is shown in Figure 1.

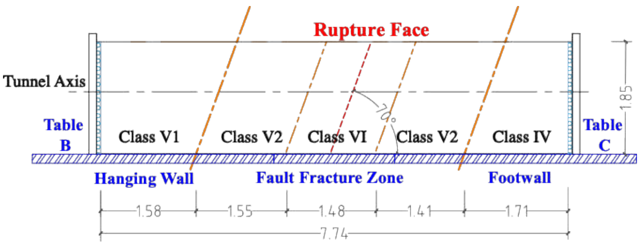

Figure 1. The front view of the shaking table model.

2 EXPERIMENTAL SETUP

2.1 Shaking table array

The tests employed the multi-point shaking table test system of the State Key Laboratory of Disaster Reduction in Civil Engineering at Tongji University. This system consists of four shaking tables: A (side table, capacity 30 tons), B (main table, capacity 70 tons), C (main table, capacity 70 tons), and D (side table, capacity 30 tons), with detailed performance parameters provided in Table 1. For this experiment, the two main tables, B and C, were used. During the test, reverse-phase strong motion-dislocation coupled ground motions were used in tables B and C to achieve simultaneous seismic and dislocation loading.

Table 1. Main Performance Parameters of the Multi-Point Shaking Table Test System

Shaking Table	A and D	B and C
Table size	6 m × 4 m	
Maximum payload	30 tons	70 tons
Degrees of freedom	3 (vertical, lateral, longitudinal)	
Max displacement	X/Y： ±500 mm	
Max velocity	X/Y： ±1000 mm/s	
Max acceleration	X/Y： ±1.5 g	
Operating frequency range	0.1–50 Hz	
Max overturning moment	200 ton·m	400 ton·m

2.2 Model container

This test employed a specifically developed model container designed to meet the requirements for simulating strong seismic motion–dislocation coupling. The main structure of the model box consists of two side rigid boxes accommodating the hanging wall and footwall of the model fault, and shear frames accommodating the model fault fracture zone. Flexible rubber is used as the connecting material between the frames. Bolt holes matching the shaking table surface are designed at the bottom of the two side rigid boxes, allowing the shaking table to serve as the input source for the strong seismic motion–dislocation coupled loading applied to the two side rigid boxes.

2.3 Similitude relation

According to the Buckingham π theorem, for a physical system involving *n* physical quantities where the dimensions of *k* quantities are mutually independent, the functional relationship among these physical quantities can be expressed in terms of *n-k* independent similarity criteria:

$$\Pi(\Pi_1, \Pi_2, \ldots, \Pi_{n-k}) = 0 \qquad (1)$$

Geometry, acceleration, and elastic modulus were selected as the mutually independent fundamental physical quantities. Taking into account the limitations of the shaking table dimensions and the need to reserve sufficient space for sensor deployment, the geometry scale ratio of the model was selected as $c_L = 40$. Based on the Buckingham π theorem, similitude relations used in the tests were derived, as shown in Table 3.

This study focuses on the dynamic response of the tunnel structure and its surrounding rock under the simultaneous action of strong earthquakes and fault dislocation, involving the interaction between the tunnel and the surrounding rock, as well as the ability of the tunnel structure to resist damage under load. Correspondingly, the key challenges in the similarity ratio design for this test are twofold: (a) In the elastic stage, the ground-structure relative stiffness ratio α (Yu and Yuan, 2018) and the surrounding rock-fault relative stiffness ratio β in the model should be consistent with those in the prototype, i.e., $c_\alpha = 1$, $c_\beta = 1$; (b) At the critical point of failure, the strength of the tunnel structure in the model should strictly satisfy the similarity ratio requirements compared to that in the prototype.

$$\alpha = \frac{E_\mathrm{s} r (1-\nu_\mathrm{l}^2)}{E_\mathrm{l} I_\mathrm{R} (1+\nu_\mathrm{s})} \qquad (2)$$

Where E_s and ν_s are the elastic modulus and Poisson's ratio of the ground, respectively, ν_l is the Poisson's ratio of the structure, and *r* is the average radius of the prototype tunnel.

$$\beta = \frac{E_\mathrm{r}}{E_\mathrm{f}} \qquad (3)$$

Where E_r is the elastic modulus of the surrounding rock, and E_f is the elastic modulus of the fault.

Table 2. Similitude relations used for the tests.

Item	Symbol
Geometry	$S_L = 40$
Acceleration	$S_{\square} = 0.75$
Elastic modulus	$S_{\square} = 48$
Unit weight	$S_\rho = S_E \cdot {S_L}^{-1} \cdot {S_a}^{-1}$
Mass	$S_{\square} = S_E \cdot {S_L}^{2} \cdot {S_a}^{-1}$
Strain	$S_\varepsilon = 1$
Stress	$S_\sigma = 1$
Velocity	$S_\upsilon = {S_L}^{\frac{1}{2}} \cdot {S_a}^{\frac{1}{2}}$
Time	$S_{\square} = {S_L}^{\frac{1}{2}} \cdot {S_a}^{-\frac{1}{2}}$
Frequency	$S_{\square} = {S_L}^{-\frac{1}{2}} \cdot {S_a}^{\frac{1}{2}}$

2.4 Model rock and model tunnel

Based on direct shear tests to control the shear strength and internal friction angle of the surrounding rock model materials, this study selected mixtures of quartz sand, fly ash, and CMC (Sodium carboxymethyl cellulose) solution in varying proportions. The target density was achieved by adjusting the compaction during the placement process to simulate the surrounding rock of the hanging wall, footwall, fault fracture zone, and core area, respectively.

According to the prototype engineering design data, the secondary lining of the tunnel uses C40/50 reinforced concrete, and the inverted arch filling uses C20/25 concrete. Based on preliminary material performance tests to control tensile strength and compressive strength, this test prepared a mixed slurry using varying proportions of high-strength gypsum, low-strength gypsum, barite powder, river sand, and water, and then poured it stepwise into specially designed molds. The process of casting and curing of model segments is shown in Figure 2. A calculated number of aluminum wires with specific diameters were bound to equivalently represent the reinforcement mesh. This approach allows for the refined simulation of the tunnel, which incorporates ductile structural designs such as segmented sections and joints with variable stiffness.

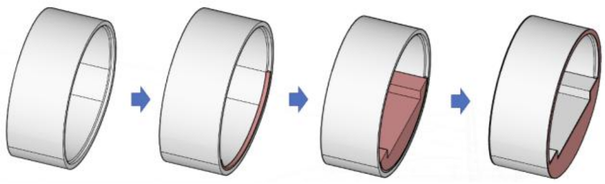

(a) Tunnel casting process

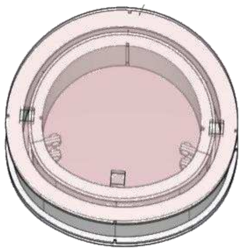

(b) Formwork assembly for secondary lining casting

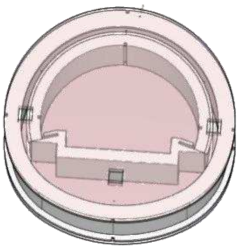

(c) Formwork assembly for invert-fill casting

(d) Batch-wise outdoor air-drying of the model segments

(e) Indoor curing of the model segments

Figure 2. The process of casting and curing of model segments.

Two tunnel models were placed parallel within the shaking table test setup (Figure 3): one is a conventional segmental tunnel (hereinafter referred to as “Tunnel A”), which was assembled directly from model segments fabricated through the aforementioned process; the other is a novel ductile tunnel (hereinafter referred to as “Tunnel B”). Compared to Tunnel A, Tunnel B incorporates an additional support system—comprising “spatial trusses + W-shaped steel strips + NPR anchor cables”—at the location corresponding to the core of the active fault zone.

As for the preparation of the model novel ductile support system (Figure 4), first, the model of the double-layer spatial truss was 3D-printed using resin material, and the W-shaped steel strip was secured to the truss. Then, components such as the constant-resistance sleeve, constant-resistance body, and the anchor cable itself were also 3D-printed with resin and assembled onto the W-shaped steel strip (Tao et al., 2024). In the double-isolation double-control model tunnel, the above-described novel ductile support system was installed on the outer side of the seven tunnel segments located in the fault-core zone.

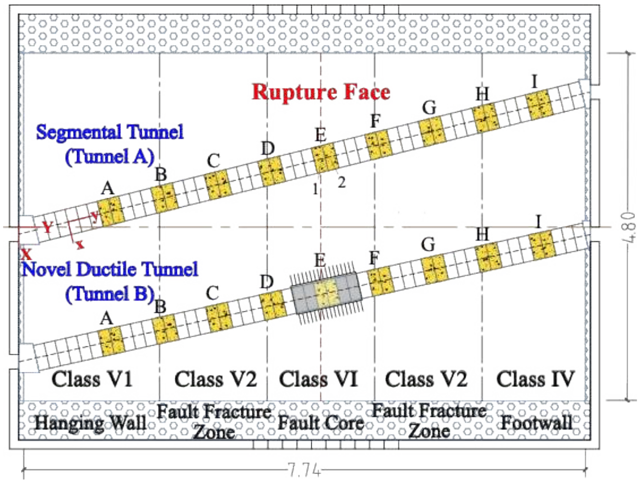

Figure 3. Plan layout of the model tunnels.

Figure 4. The model novel ductile support system.

3 SHAKING TABLE TEST PROGRAMME

3.1 Test cases

By adopting different models, input motion levels, types of input motion, and fault dislocation modes, this study established a series of test cases as shown in Table 3.

Table 3. Test cases.

Variable	Range
Model	Free-field, ground-tunnel
Input motion level	0.05 g, 0.143 g, 0.571 g, 1.0 g
Input motion category	White noise, sine wave, natural ground motion, synthetic pulse-like wave, synthetic seismic-slip coupled wave
Fault dislocation mode	Creep, stick-slip

3.2 Instrumentation

To better capture the response of the model tunnel during the test loading, nine key segment groups (A~I) were established on both the segmented comparison tunnel and the double-isolation double-control tunnel, as shown in Figure 3. Specifically: Segment Group A is located within the hanging wall surrounding rock; Group B is situated at the boundary between the hanging wall surrounding rock and the fault fracture zone; Group C is located inside the fault fracture zone on the hanging wall side; Group D is at the boundary between the fault fracture zone on the hanging wall side and the fault core; Group E is positioned within the fault core; Group F is at the boundary between the fault fracture zone on the footwall side and the fault core; Group G is located inside the fault fracture zone on the footwall side; Group H is situated at the boundary between the footwall surrounding rock and the fault fracture zone; and Group I is located within the footwall surrounding rock. Each key group consists of two segments, with the segment closer to the hanging wall numbered 1 and the segment closer to the footwall numbered 2.

The data measured during the tests and the corresponding sensors include: soil and structural acceleration (accelerometers), tunnel segment attitude (gyroscopes), tunnel diameter deformation (laser displacement sensors), lining hoop and longitudinal strain (strain gauges), surrounding rock pressure (earth pressure cells), misalignment between lining segments (push-rod displacement transducers), lateral displacement deformation of the surrounding rock (wire-draw displacement transducers), and longitudinal strain distribution within the surrounding rock (OFDR-based optical fiber strain sensors). The layout of sensors on the key tunnel segments is shown in Figure 5. A total of three layers of OFDR optical fiber strain sensors were deployed. The distance of each layer from the bottom of the model and the sensor arrangement within each layer are shown in Figure 6.

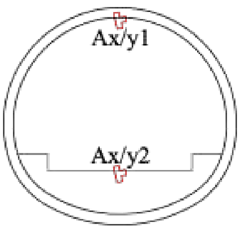

(a) Dual-axis accelerometer (at A2, B2, C2, F2, G2, H2, I2)

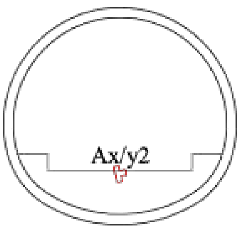

(b) Dual-axis accelerometer (at D1)

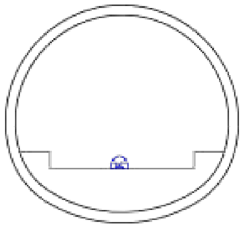

(c) Gyroscope (at D2–F1)

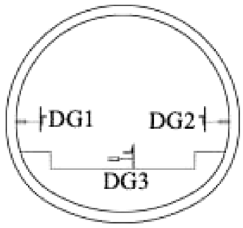

(d) Push-rod displacement transducer (at C, D, E, F, G)

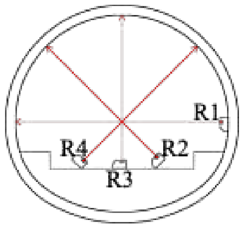

(e) Laser displacement transducer (at D2, E1, E2, F2)

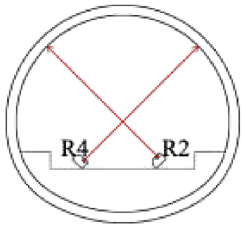

(f) Laser displacement transducer (C2, G2)

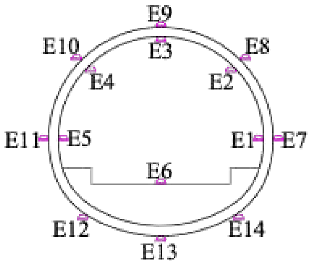

(g) Longitudinal strain gauge (at C1, D1, F1, G1)

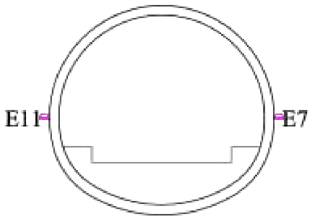

(h) Longitudinal strain gauge (at E1, E2)

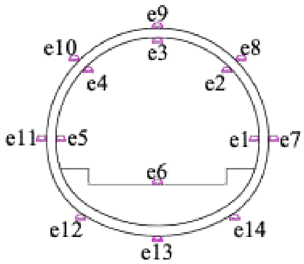

(i) Hoop strain gauge (at E1, E2)

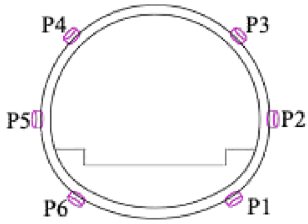

(j) Earth pressure cell (at C1, D1, E1, E2, F1, G1)

Figure 5. Key segment sensor layout diagram.

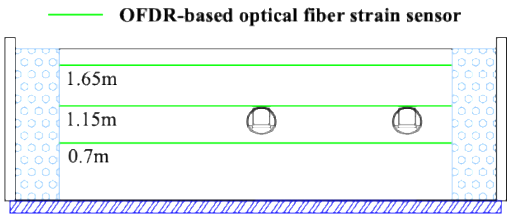

(a) Along depth

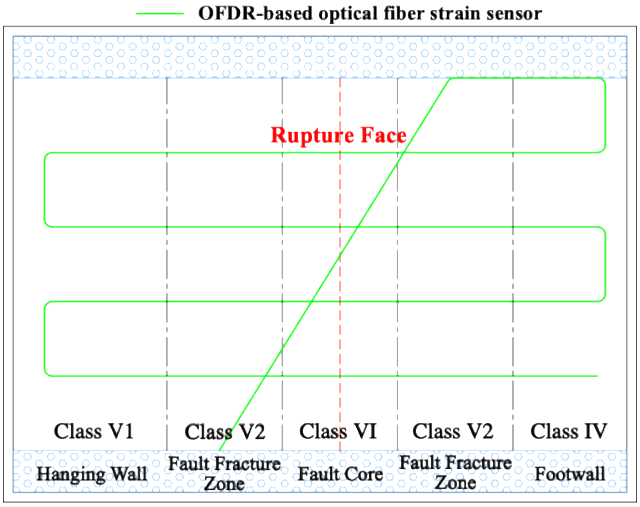

(b) In plane

Figure 6. Arrangement of OFDR optical fiber strain sensors.

4 CONCLUSIONS

(1) The multi-layer linkage coupling device, integrated with Tongji University's shaking table system, provides an effective technical means for the synchronous application of seismic shaking and fault dislocation in physical modelling.
(2) The scaled model satisfies the similitude relations for ground-tunnel relative stiffness and strength, ensuring a reasonable representation of the segmental tunnel's structural characteristics.
(3) A comprehensive test programme—covering free-field and ground-tunnel models, varied input motions, and fault dislocation modes—offers a systematic approach for investigating tunnel response under coupled excitation.
(4) The instrumentation strategy, including accelerometers, strain sensors, and OFDR-based sensing, is designed to capture key dynamic responses of the tunnel and surrounding rock.

ACKNOWLEDGEMENTS

The authors are grateful for the financial support provided by funding agency Ministry of Science and Technology of China. The project presented in this paper is supported by National Key Research and Development Program of China (2025YFE0125500).

REFERENCES

Liu, Y., Lai, J., Xin, J.P., et al. (2019). Comparison test of dynamic response characteristics of the tunnels through fault. *Rock and Soil Mechanics*, 40(12): 4693-4702. https://doi.org/10.16285/j.rsm.2018.1824

Shen, Y.S., Wang, Z.Z., Yu, J., et al. (2020). Shaking table test on flexible joints of mountain tunnels passing through normal fault. *Tunnelling and Underground Space Technology*, 98: 103299. https://doi.org/10.1016/j.tust.2020.103299

Sun, F.B., Zhao, B.M., Yang, Q.Y. et al. (2018). Calculation formula and experimental verification for quantitative setting of combined seismic joints in tunnels crossing active faults. *China Railway Science*, 39(2): 61-70. https://doi.org/10.3969/j.issn.1001-4632.2018.02.08

Tao, Z.G., Feng, Y.X., Zhao, Y., et al. (2024). Shaking table test on anti-seismic characteristics of NPR anchor cable support system for tunnel crossing faults. *Rock and Soil Mechanics*, 45(4): 939-949. https://doi.org/10.16285/j.rsm.2023.0606

Wang, S.S., Gao, B., Sui, C.Y. et al. (2015). Mechanism of shock absorption layer and shaking table tests on shaking absorption technology of tunnel across fault. *Chinese Journal of Geotechnical Engineering*, 37(6): 1086-1092. https://doi.org/10.11779/CJGE201506015

Xin, C.L., Gao, B., Yan, G.M., et al. (2016). Study on seismic failure characteristics and anti-seismic measures of tunnels crossing strike-slip faults. *Journal of Vibration Engineering*, 29(4): 694-703. https://doi.org/10.16385/j.cnki.issn.1004-4523.2016.04.017

Yu, H.T. and Yuan, Y. (2018). Review on Seismic Response Analysis and Test Methods for Long and Large Tunnels. *China Journal of Highway and Transport*, 31(10): 19-35.https://doi.org/10.3969/j.issn.1001-7372.2018.10.003

Xu, Q.W., Cheng, P.P., Zhu, H.H., et al. (2016). Experimental study and numerical simulation on progressive failure characteristics of the fault-crossing tunnel surrounding rock. *Chinese Journal of Rock Mechanics and Engineering*, 35(3): 433-445. https://doi.org/10.13722/j.cnki.jrme.2015.0604

Xu, T.Q. and Li, S.G. (2022). Research on Influence of Reverse Fault Dislocation on Tunnel Structure. *Railway Standard Design*, 66(6): 117-122. https://doi.org/10.13238/j.issn.1004-2954.202103020013

Zhang, X., Shen, Y.S., Chang, M.Y., et al. (2023). Shaking table test research on seismic damage and failure of tunnel segmental lining crossing multiple rupture surfaces. *Chinese Journal of Rock Mechanics and Engineering*, 42(9): 2237-2252. https://doi.org/10.13722/j.cnki.jrme.2023.0387